Supplementary information

Flow-gel approach enables rapid extraction of pure magnesium phase from seawater

Pravalika Butreddy[a], Andrew Ritchhart a, Qingpu Wang[b] , Heather Job[a], Maria Sushko,[a] Jaehun Chun[a], and Elias Nakouzi[*a]

1. Experimental Section:

Chemicals. Agarose (Type I, low EEO, Sigma Aldrich), sodium hydroxide (NaOH, anhydrous, ≥ 97%, Sigma-Aldrich), and model seawater salt mix (Instant Ocean) were used as received. All solutions were prepared using ultrapure Type I (resistivity, 18.2 MΩ.cm) water filtered by a PURELAB Flex (Elga) water purification system.

Gel preparation and separation experiments. A gel solution (3.0 wt%) was prepared by adding 0.3 g agarose powder to 9 mL deionized water and 1 mL NaOH (10 M) solution under continuous stirring in a hot water bath (90 °C) until the gel became homogenous. Subsequently, this NaOH-containing gel solution was transferred into a petri dish (100mm x 15mm, sterile, polystyrene, Fisherbrand) and allowed to cool to room temperature for the agarose gelation. A 10 mL instant seawater solution was used for the preliminary experiments performed at various timescales, 2 min, 2 hours, and 24 hours, both under and without shaking. The white precipitates that formed above the gel layer were carefully collected after centrifugation (10000 rpm for 7 min) and washed using deionized water twice. For the bulk mixing, 10mL of the instant seawater solution was mixed with 10mL of 1M NaOH solution under constant stirring, and the precipitate was collected after 24 hours. These precipitates were also washed using deionized water twice and collected using centrifugation.

Construction of the flow-gel device. We constructed the flow-gel device by custom-designing a prototype using the onshape CAD software. A 3D printer (Original Prusa i3) was used to make the prototype using standard PLA filament. This prototype has a channel length of 15.2 cm, a width of 2.5 cm, and a height of 2 cm (Figure S1). It also contains an inlet and outlet (8mm diameter) to allow the feedstock to flow on the gel layer. We then glued a plastic barbed tube fitting to the inlet of the prototype using an epoxy adhesive (J-B Weld ClearWeld). We avoided using the tube fitting at the outlet (Figure S2) to prevent undesired precipitation accumulation and clogs.

Characterization of the precipitate samples. An orbital shaker (VWR, DS-500E) was used for the separation experiments under shaking at a constant speed of 90 rpm. These precipitates, after washing, were redispersed in deionized water and later drop-cast onto a glass slide for imaging using a Keyence VHX 7000 Optical Microscope. The redispersed precipitates were drop-cast separately onto silicon wafers. They were later imaged using a ThermoFisher Scientific Apreo 2 scanning electron microscope (SEM) equipped with an Oxford Instruments energy dispersive spectroscopy (EDS) detector, which was used for the elemental analysis.

The dried precipitates collected from the separation experiments were first measured using an analytical balance (Sartorius, BCE224i-1S). Further, Powder X-ray diffraction (XRD) analysis was performed using Cu Kα radiation (λ = 1.54 Å) on a Bruker D8 advance X-ray diffractometer at a step width of 0.02 deg with the start and stop angles being 25° and 65° respectively. Fourier transform infrared (FTIR) spectra of the precipitates were acquired using a Bruker Alpha II spectrometer operating in attenuated total reflection mode at room temperature. The FTIR spectra were recorded for a wavenumber range of 4000–500 cm^{-1} with a

spectral resolution of 4 cm^{-1}. TGA Analysis was performed on the precipitate powder samples using a Netzsch STA 449 F1 Jupiter thermal analysis instrument. The TGA analysis was performed under a nitrogen environment in an Alumina DTA crucible at a ramp rate of 10 °C/min from 25 – 900 °C. The elemental composition of the precipitates was confirmed using a PerkinElmer Optima 8300 Dual View Inductively Coupled Plasma-Optical Emission Spectrometer (ICP-OES) with a PerkinElmer S-10 auto-sampler interface. For these analyses, 1 mg of the precipitate samples were digested in a 70% nitric acid and was diluted with ultrapure water by a factor of 20 to reach the final acid concentration of about 2%. All the samples were filtered through a 0.22 µm filter (VWR syringe filter, Nylon, 25 mm) in preparation for the ICP-OES analysis.

2. Reaction-diffusion-advection model

To further understand a competition between advection and precipitation, a scaling argument can be used (Figure S7d). A timescale associated with precipitation is scaled as $\tau_{rxn} \sim 1/kC_{A0}$. Here k is a rate coefficient for precipitation based on a simple kinetic model, $-\frac{dC_B}{dt} = kC_{A0}C_B$, where C_{A0} is a bulk concentration of A assuming no mass transfer barrier to the gel interface. A time scale for advection is $\tau_{conv} \sim l/V_{A0}$ where l and V_{A0} denote a characteristic dimension of container associated with advection of A and the bulk velocity of A. An "immediate" precipitation corresponds to $\tau_{rxn} \ll \tau_{conv}$ where a relative importance between advection and diffusion is critical for the process. In this case, k can be approximated as V_{A0} (i.e., $N_{RD} = nV_{A0}L/D$) that would be obtained from the volumetric flow rate and a gel surface exposed to the flow. In the opposite limit, $nk \rightarrow lkC_{A0}$ considering the simple kinetic model. This will lead to $N_{RD} = (l/L)\tau_{diff}/\tau_{rxn}$ involving a geometric factor l/L ($\tau_{diff} = L^2/D$), showing that N_{RD} represents a relative importance of diffusion compared to precipitation in this limit. N_{RD} can be thus identical to Karlovitz number (i.e., an inverse of Damköhler number).

The simple model can be easily extended to a case having two competing cationic reactants A_1 (e.g., Mg^{2+}) and A_2 (e.g., Ca^{2+}) brought by flow. Considering contributions from both A_1 and A_2 for the balance between diffusional flux and advectional/reactional flux at $z = L$, the "immediate" precipitation can lead to $N_{RD}^1 = n^1V_0L/D$ and $N_{RD}^2 = n^2V_0L/D$ where n^1 and n^2 denote a molar ratio of B to A_1 and that of B to A_2 involved in precipitation, respectively. Note that a bulk velocity of flowing fluid V_0 can be used to represent bulk velocities for A_1 (V_{A10}) and A_2 (V_{A20}), assuming no mass transfer barrier to the gel interface. This is based on a similar scaling argument for both A_1 and A_2; $1/(k^1C_{A10}) \ll l/V_0$ and $1/(k^2C_{A20}) \ll l/V_0$ where k^1 and k^2 are rate coefficients for precipitation involving A_1 and A_2 respectively, based on the same kinetic model. In case $n^1 = n^2$ (e.g., $Mg^{2+}\cdots OH^-$ vs. $Ca^{2+}\cdots OH^-$), $N_{RD}^1 = N_{RD}^2$. Following a similar rationale for an opposite limit where a competition between two precipitation reactions and diffusion is critical, we can define two N_{RD} values, $N_{RD}^1 = (l/L)\tau_{diff}/\tau_{rxn}^1$ and $N_{RD}^2 = (l/L)\tau_{diff}/\tau_{rxn}^2$, where $\tau_{rxn}^1 \sim 1/k^1C_{A10}$ and $\tau_{rxn}^2 \sim 1/k^2C_{A20}$. The scaling for two N_{RD} values implies that $N_{RD}^1 \gg 1$ but $N_{RD}^2 \ll 1$ is a condition to achieve a complete separation of cation A_1 from mixture of cations A_1 and A_2 using the flow-gel approach, corresponding to $\tau_{rxn}^2/\tau_{rxn}^1 \gg 1$. This scaling based on the simple model also suggests that tailoring the diffusion within the gel is needed because a smaller τ_{diff} will not facilitate the separation due to decreasing N_{RD}^1.

3. Supporting figures

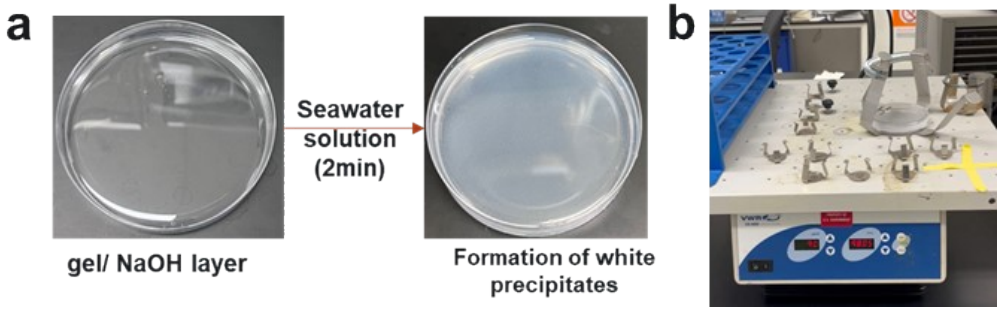

Figure S1. Petri dishes from the **(a)** without shaking versus **(b)** shaking preliminary experiments.

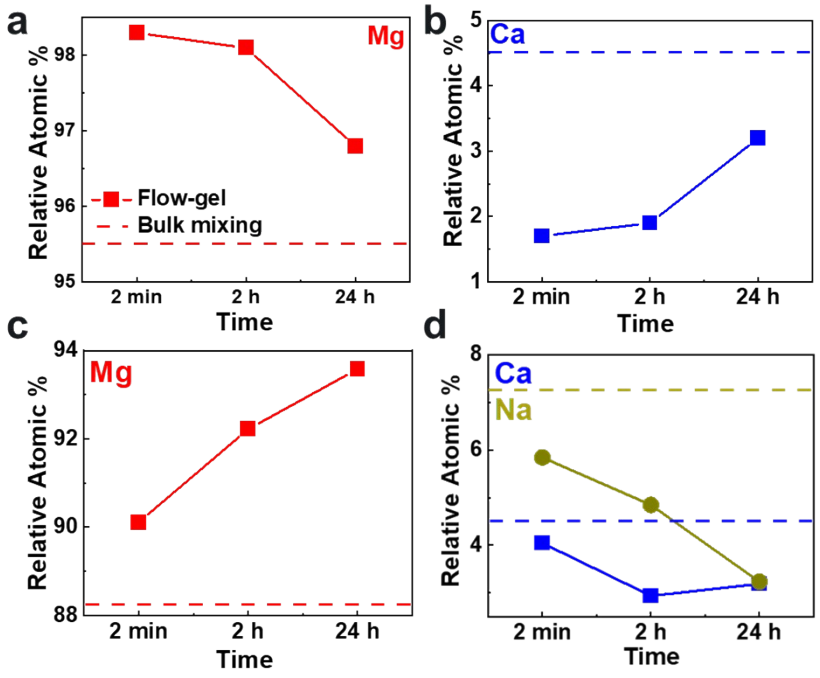

Figure S2. Data obtained from the separation experiments under shaking. (a, b) EDS and (c, d) ICP-OES analyses showing Ca, Mg, and Na at% in the precipitates and comparison with the bulk mixing method (dashed lines)

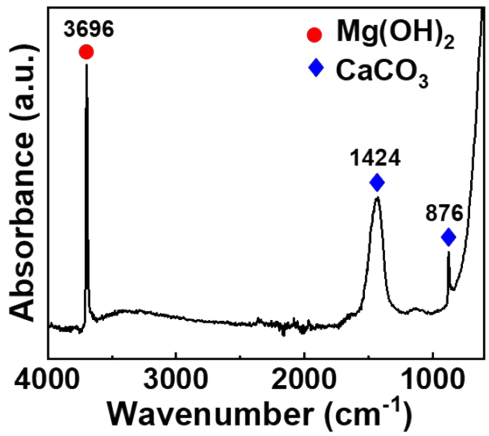

Figure S3. FTIR spectrum of the products from bulk mixing.

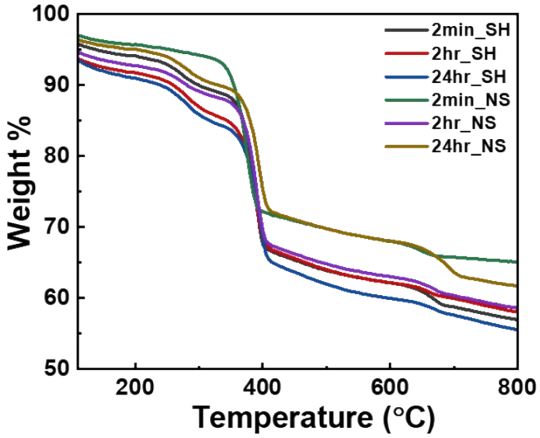

Figure S4. TGA analysis of the precipitates recovered from shaking (SH) and without shaking (NS) at 2 minutes, 2 hours, and 24 hours.

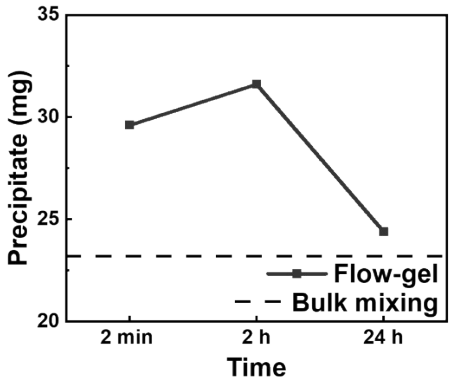

Figure S5. Mass of the precipitates recovered from the experiments without shaking

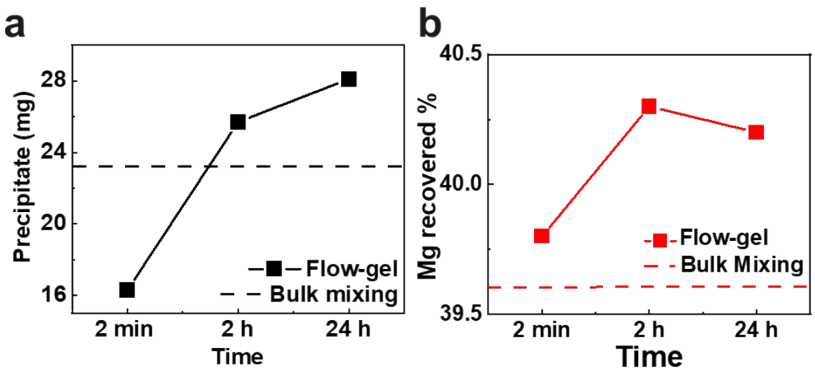

Figure S6. Data obtained from the separation experiments under shaking. (a) Mass of the precipitates recovered, (b) % Mg recovered from the precipitates.

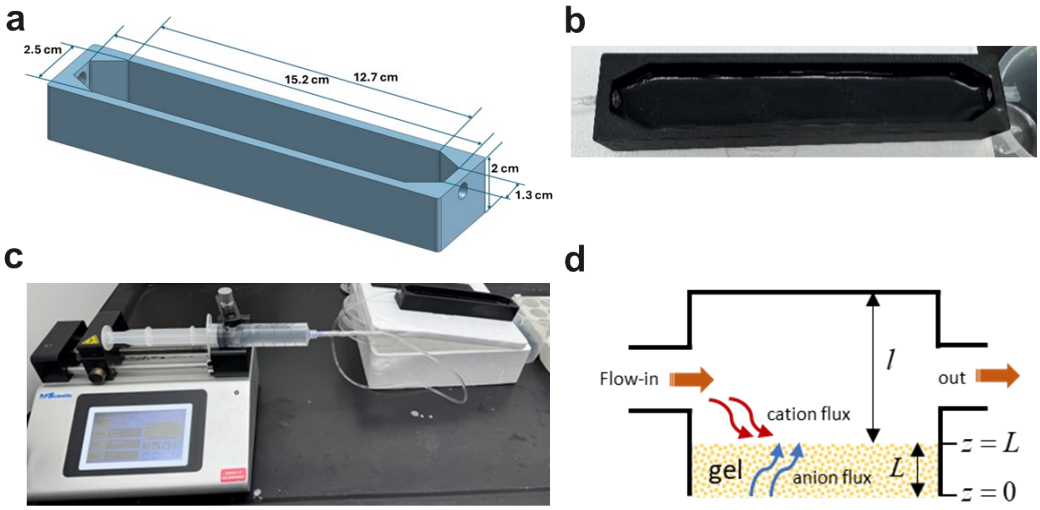

Figure S7. (a) Schematic of the flow-gel device, (b) Photograph of the flow-gel device with the gel/NaOH layer and under no flow condition, (c) Photograph of the flow-gel device placed at an angle of ~10° with the syringe pump, (d) Schematics for the simple model

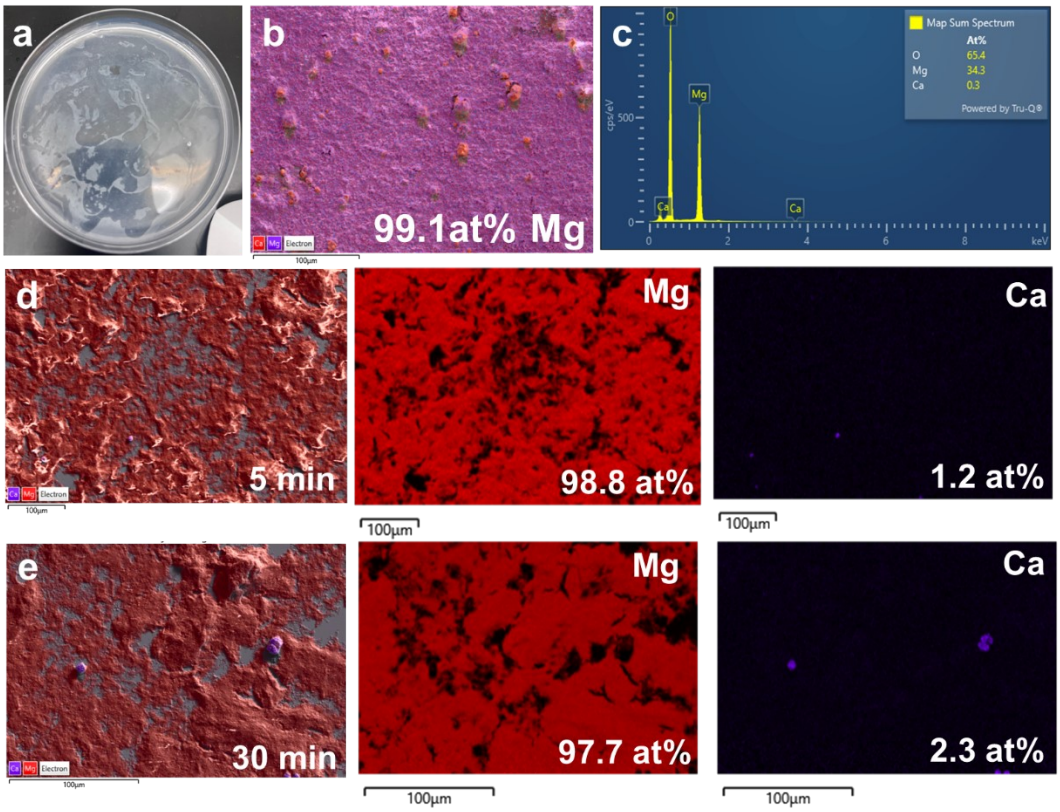

Figure S8. (a) Photograph of the petri-dish experiment using a lower NaOH (0.1 M) concentration loaded in the agarose (0.4%) gel layer and the feedstock solution containing 841 mg/L $MgCl_2$ and 323 mg/L $CaCl_2$, and the corresponding (b) EDS map (Note: magnesium is purple in color and calcium in red), (c) EDS spectrum of the precipitates collected; (d) & (e) EDS maps of the precipitates collected at 5 minutes and 30 minutes with a slightly different seawater concentrations (8571mg/L NaCl, 841 mg/L $MgCl_2$, 323 mg/L $CaCl_2$ and 7.5 mg/L $SrCl_3$).